SANDIA REPORT

SAND2001-2160
Unlimited Release
Printed July 2001

Breakdown in ZnO Varistors by High Power Electrical Pulses

Gordon Pike

Prepared by
Sandia National Laboratories
Albuquerque, New Mexico 87185 and Livermore, California 94550

Sandia is a multiprogram laboratory operated by Sandia Corporation, a Lockheed Martin Company, for the United States Department of Energy under Contract DE-AC04-94AL85000.

Issued by Sandia National Laboratories, operated for the United States Department of Energy by Sandia Corporation.

Available to DOE and DOE contractors from
U.S. Department of Energy
Office of Scientific and Technical Information
P.O. Box 62
Oak Ridge, TN 37831

Telephone: (865)576-8401
Facsimile: (865)576-5728
E-Mail: reports@adonis.osti.gov
Online ordering: http://www.doe.gov/bridge

Available to the public from
U.S. Department of Commerce
National Technical Information Service
5285 Port Royal Rd
Springfield, VA 22161

Telephone: (800)553-6847
Facsimile: (703)605-6900
E-Mail: orders@ntis.fedworld.gov
Online order: http://www.ntis.gov/ordering.htm

SAND2001-2160
Unlimited Release
Printed July 2001

Breakdown in ZnO Varistors by High Power Electrical Pulses

Abstract

This report documents an investigation of irreversible electrical breakdown in ZnO varistors due to short pulses of high electric field and current density. For those varistors that suffer breakdown, there is a monotonic, pulse-by-pulse degradation in the switching electric field. The electrical and structural characteristics of varistors during and after breakdown are described qualitatively and quantitatively. Once breakdown is nucleated, the degradation typically follows a well-defined relationship between the number of post-initiation pulses and the degraded switching voltage. In some cases the degraded varistor has a remnant 20 μm diameter hollow track showing strong evidence of once-molten ZnO. A model is developed for both electrical and thermal effects during high energy pulsing. The breakdown is assumed to start at one electrode and advance towards the other electrode as a thin filament of conductive material that grows incrementally with each successive pulse. The model is partially validated by experiments in which the varistor rod is cut at several different lengths from the electrode. Invariably one section of the cut varistor has a switching field that is not degraded while the other section(s) are heavily degraded. Based on the experiments and models of behavior during breakdown, some speculations about the nature of the nucleating mechanism are offered in the last section.

Contents

Breakdown in ZnO Varistors by High Power Electrical Pulses

Introduction

Varistors are electronic devices with highly nonlinear current-voltage relationships. The functional dependence of current on voltage is symmetrically bipolar and an inherent property of the polycrystalline semiconductor from which it is made. At small applied electric fields, varistors are insulating; but at a fairly well-defined, higher field, they switch to conducting and maintain a nearly constant field over many decades of current. Most commercial, military, and Sandia application varistors are based on polycrystalline, semiconducting ZnO with a variety of other oxide additives typically in the molar range of 100 parts per million to several percent. Their main application is in electrical circuits to limit or regulate the voltage that can be applied to other devices or components. While it is not unusual for all varistors to operate with current densities of 10^{-3} to 10 A/cm^2, some Sandia applications also require unusually high electric fields near 40 kV/cm. With these high power conditions, it is perhaps not surprising that small flaws in the varistor result in breakdown, or a large irreversible change in their electrical and sometimes structural properties. The purpose of this report is to document experiments and model calculations that address the nature of varistor breakdown in the regime of high current density, high electric field, and short pulse widths. Comments on the initiation mechanism are offered at the end of the report.

Materials and Electrical Tests

All varistors in this study used ZnO as the nonlinear material. Most of the polycrystalline ZnO elements were fabricated by sintering ZnO powder produced by the Sandia Chem-Prep process[1,2]. In this process, a chloride solution containing all cation components of the varistor, except bismuth and sodium, is prepared. NaOH solution is added to form a homogeneous hydrous oxide slurry, followed by the addition of oxalic acid to convert the slurry to an oxalate co-precipitate by a dissolution-re-precipitation reaction. A water wash, vacuum drying, and a two hour calcine at 600ºC yields a "zincite" powder. Bismuth nitrate solution is added to a re-slurry of the zincite powder. This causes hydrated Bi compounds to precipitate on the powder particle surfaces, and these are converted to a layer of Bi_2O_3 by subsequent calcining at 400ºC for two hours. Finally, sodium oxalate is added in solution to a slurry of the Bi-coated zincite powder and freeze-dried to leave a layer of oxalate on the particles. Calcining again at 400ºC for two hours dopes the powder with about 300 ppm sodium, which has been found to be beneficial for improving reliability under high power pulses.

The powder is pressed into a cylindrical mold, then sintered at 732ºC. A pattern of opposing silver paint electrodes is typically applied to the flat surfaces of the cylindrical sintered wafer so the material can be electrically tested before further fabrication. The wafer is then cut along sectors, and cylindrical rods of varistor material are cored-drilled parallel to the flat wafer surface. Kovar electrodes are attached to each end of the cut rod using a thin silver-loaded epoxy cloth preform. Then the entire varistor is surface ground to the desired diameter. Some of the varistors were subsequently encapsulated in Epon 828 epoxy containing a high density of hollow glass microballoons.

Electrical pulse testing was performed using a high voltage tester of Sandia design as shown schematically in Figure 1. The tester is intended to measure the voltage across the varistor at a fixed current[3] determined by the value of the current limiting resistor. Although not shown in the figure, there were actually two resistors available in any given test series. This permitted the two-point determination of the nonlinearity coefficient,

$$\alpha \equiv \Delta \ell n(J)/\Delta \ell n(E), \quad (1)$$

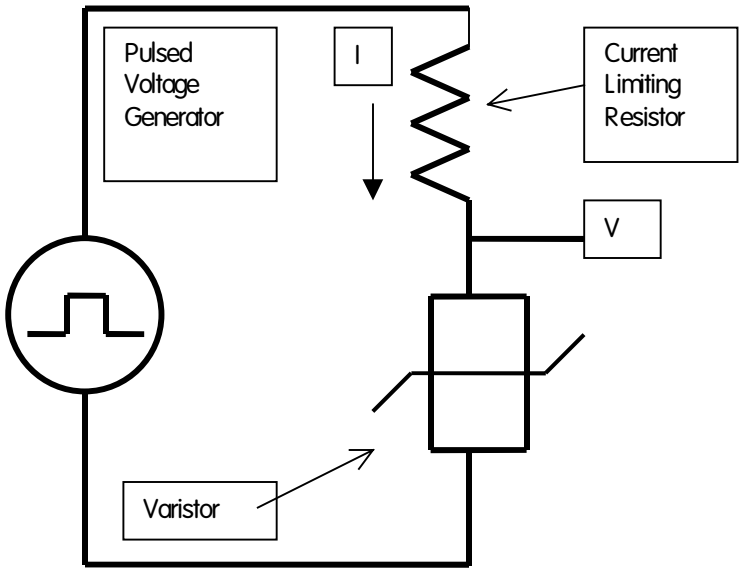

Figure 1. Schematic diagram of the electrical tester for varistors. The generator voltage is several times higher than the varistor's limiting voltage, thus the circuit is nearly constant current.

where J is the current density and E the electric field. The current pulse is approximately 10 μs long with a rise time of about 1 μs. Pulses were applied about 20 seconds apart. Typically, a high/low current pulse pair would be applied at the beginning of a testing sequence to measure the nonlinearity coefficient, which was usually 20 or slightly larger. Subsequent pulses would be only high current pulses to determine the reliability of the varistors, and to examine the breakdowns under constant current conditions when they did occur. Pulsing was done to varying degrees of electrical breakdown to enable structural examination of the stages. During the electrical testing, all varistors were immersed in a bath of Fluorinert FC-77 (3M Corp.) to suppress surface arcing.

Pulse Test Results – Electrical

The main purpose of the electrical tests was to determine the electrical performance reliability of the varistors. Twenty-five pulses were standard for these tests, but some samples were tested for hundreds of pulses. Many of the varistors survived the electrical reliability tests with no discernable changes in properties. However, the topic of this report is the breakdown behavior of those varistors that did not survive the testing without change. Because the pulse tests were conducted as part of a Sandia varistor development program, the samples were fabricated with several deliberate process variations, at several sites, and from several chemical sources. While there were often large variations in reliability among different process lots, there was a very consistent pattern for the electrical breakdowns that did occur.

Varistors that suffered a permanent change in their electrical properties almost always exhibited two regimes. First there was a regime in which the measured voltage appeared to be constant within the noise-limited precision of the measurement which was roughly ±0.5%. The number of pulses in this regime was quite variable from lot to lot, and among varistors within the same lot. Of course, this was the only regime observed for varistors which passed the reliability tests. Breakdown was always observed to be a decrease in the measured pulse voltage. Within several pulses of the first noticeable decrease, a new trend was established. Each subsequent pulse caused a decrease in voltage that was a constant fraction of the original voltage. For varistors with switching fields of 40 kV/cm receiving current pulses of 11 A/cm^2, each pulse in the breakdown regime would cause an incremental decrease of about 4% of the original voltage.

Because of this common behavior, it is possible to overlay curves of measured voltage, normalized by their original value, as a function of number of pulses, adjusted for the first noticed voltage decrease, to get a single curve for many varistors. Of course, the slope of the curve in the breakdown regime depends strongly on the pulse parameters, and to a lesser extent on the process lot. An example of a single curve is shown for six varistors from 3 similar process lots in Figure 2. Each of these varistors began to exhibit a voltage decrease at different

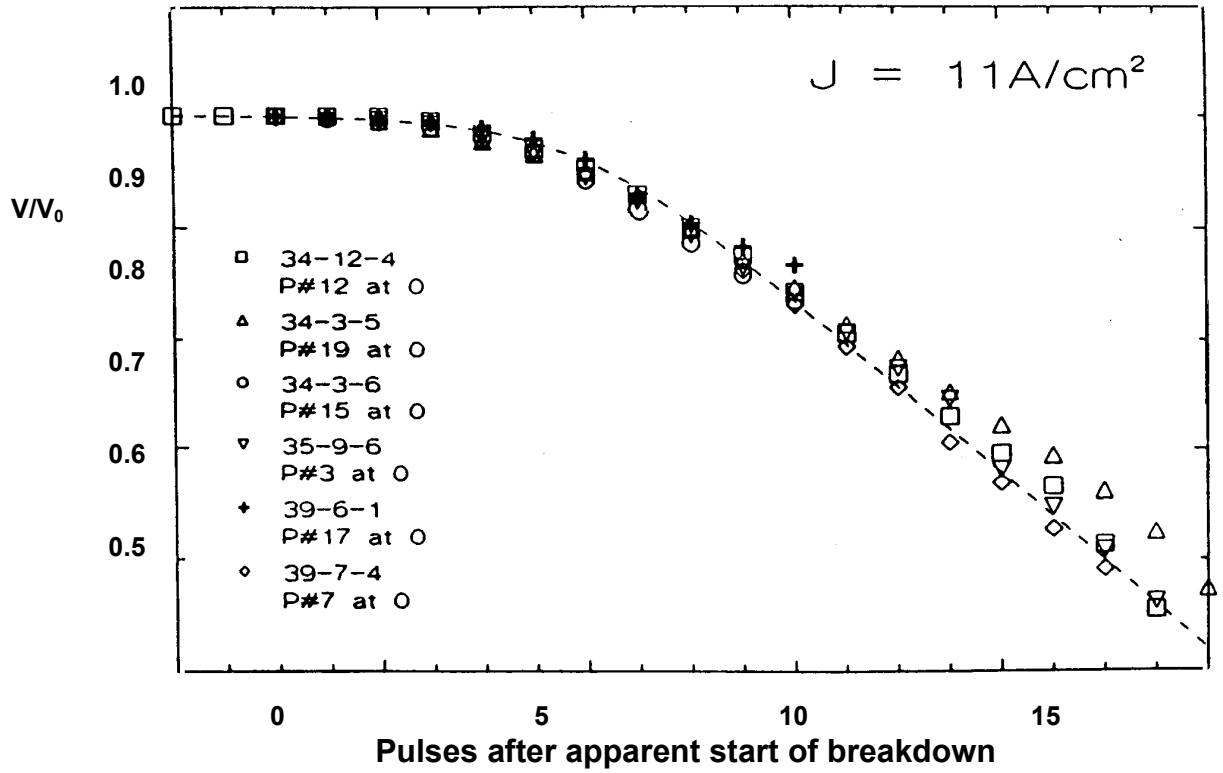

Figure 2. Electrical properties of ZnO varistors in breakdown. The ordinate scale shows the voltage across each varistor subjected to a series of constant current pulses. The value is normalized by the voltage of the first pulse, V_0. Each of the six varistors had an apparent start of breakdown at a different pulse number, but the curves were made coincident by translating them along the abscissa. The actual pulse number corresponding to pulse zero in the graph is indicated in the legend.

pulse numbers, but it is possible to translate each curve along the pulse number axis to create a near correspondence for all. If the number of pulses in the apparently normal, original voltage state are subtracted from the total number of pulses, this yields the number of pulses, P_a, received in the apparent breakdown regime. An empirical fit to the breakdown curves is given by

$$V/V_0 = 1 - 0.06\ell n\{1 + \exp[(2/3)(P_a - 6)]\}. \quad (2)$$

The form of this fitting equation was chosen because it has the correct limiting behavior early and late in the breakdown characteristics.

Pulse Test Results – Structural

A few of the varistors that had electrical breakdowns were found to have holes on the electrode surfaces of the ZnO. These holes were first noticed because of small holes at the periphery of the silver-loaded epoxy preforms that were connected to the ZnO holes by a black track in the preform. An example of a hole in the ZnO electrode surface is shown in Figure 3. There is evidence not only of a hole, but also of once-molten flow on the surface. Frequently these samples have a single crack which passes through the hole. When the crack is forced opened, an obvious track is exposed along the crack surface as seen in Figure 4. Both the hole and the track are typically 20 μm in diameter. The tracks are hollow, their surfaces are glassy and occasionally they show a radial crystalline re-growth region as shown in Figure 5. The hole and track structures in the varistors strongly indicate that a filament had formed with temperatures high enough to melt the ZnO locally. It was also hot enough to produce a vapor pressure sufficient to force much of the molten ZnO out through the electrode, through the preform under the solid Kovar endcap, and out into the Fluorinert.

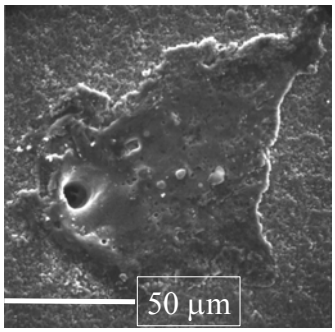

Figure 3 – Example of an electrode hole caused by high voltage breakdown.

Figure 4. Example of an internal track caused by high voltage breakdown.

The extent of track penetration into the bulk of varistor rods, without fracture or surface tracks, was probed by

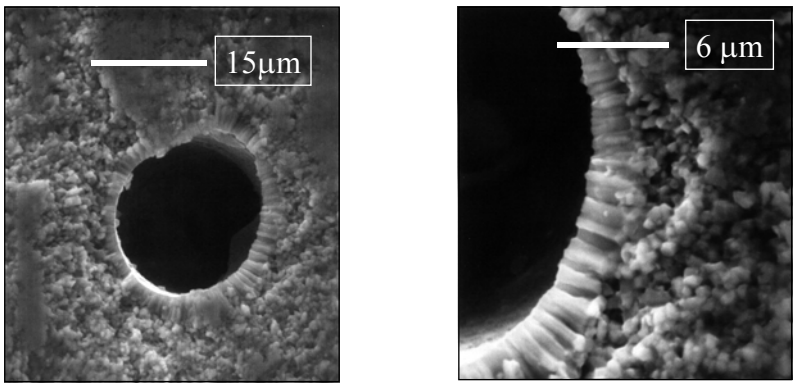

Figure 5. Example of radial recrystallization inside a breakdown track.

cutting the rods at
various lengths. Initially the rods were just cut in half. Later, guided by results of a model calculation, two badly degraded rods were cut into thirds. Only two rods of the 21 cut for track examination showed a track both starting in the electrode surface and passing entirely through the cut piece. One track ran through a half-length, the other through a third. Both samples had been degraded to $V/V_0 = 0.59$. Rods that had fractures or surface tracks did not follow the single curve electrical breakdown and were not sectioned.

Another occasional feature of electrically degraded varistors were 50 μm pits in the electrode or cut surfaces that were ringed by larger halos of Bi-rich material as determined by EDS (energy dispersive spectrometry) in the scanning electron microscope (Fig. 6). EDS also indicated qualitatively high concentrations of silicon at the bottom of the pits. These halo pits did not appear to be part of a penetrating hollow track. Of the 21 cut samples examined, three showed these Bi-halos on one electrode surface and three had them on interior cut surfaces.

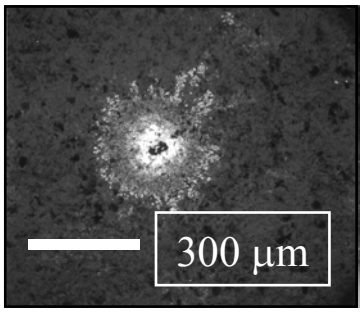

Figure 6 - A backscattered electron image of a Bi halo.

Some varistors had more obvious structural damage in the form of tracks along the cylindrical surface. These surface tracks did not always extend to an electrode surface, and it was common to see a surface track emerge from and re-enter the cylindrical surface. Electrically, these varistors did not follow the well-defined, single curve breakdown. Instead the rate of voltage decrease per pulse was up to three times faster. An interesting hybrid is shown in Figure 7 for varistor GB136B 60-1 A1. This varistor had a hole in one electrode, a short surface track just below that electrode, and holes in both halved surfaces after it was cut. Notice that the electrical properties change more rapidly than standard at first, then join and follow the common, single curve for the remainder of the pulse testing. The interpretation is that the rapid changes were associated with the surface track, and that the single curve behavior occurred after the track re-entered the bulk of the varistor.

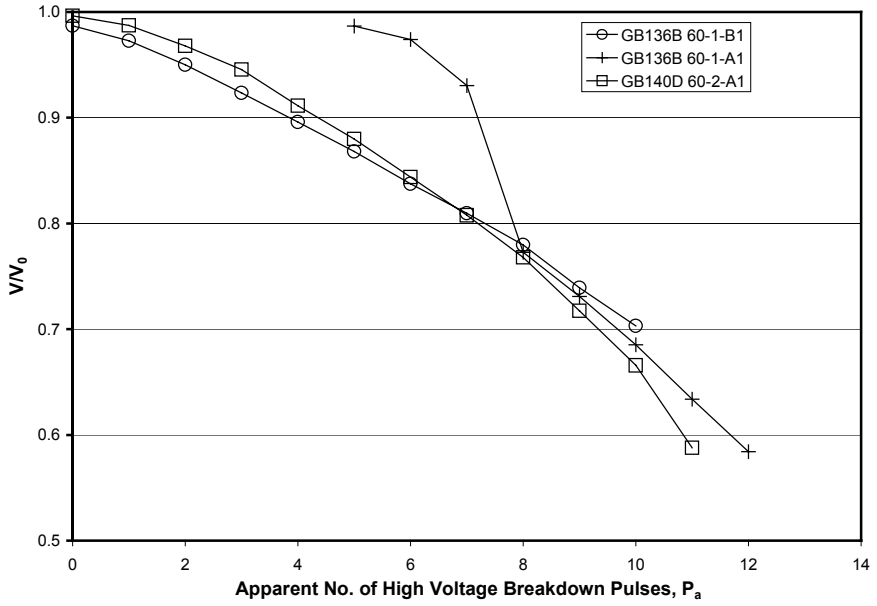

Figure 7. Comparison of electrical breakdowns between varistors with and without a surface breakdown track.

Finally, I note that while fractures and tracks remnant of high temperature filaments

in the varistors are dramatic signs of electrical breakdown, many varistors showed none of these features after breakdown. For a few varistors, an intense topographical examination was made of electrode and cut surfaces using optical and electron beam microscopy without discovering tracks or other breakdown remnant features. Nevertheless, subtle changes of grain texture or intergranular phases may have been missed. Also, even in the presence of a high temperature filament, the major structural changes may have been suppressed because of the strength of the sintered ceramic body.

Breakdown Model

In this section, a model is presented to explain the essential electrical and structural features of ZnO varistors in the breakdown regime during pulse testing. Although the model does not explicitly address the materials issues associated with the initiation of breakdown, it does offer some insights. The essential assumption of the model is that the voltage decrease is due to a single conductive filament that forms at one of the electrodes and grows in length towards the opposite electrode with each applied pulse.[4] Figure 8 shows the concept. The varistor length is L and the filament length is L_f. In the pulsed, high current condition, the varistor material everywhere, except in the conductive filament, obeys the standard approximate relationship of $J = pE^{\alpha}$, where α is the nonlinearity coefficient and p is a constant. Because the filament is conductive, the voltage at the bottom of the filament is the same as the voltage on the top electrode. This makes the electric field in the column below the filament higher than the electric field in the remainder of the varistor[5]. With $\alpha \sim 20$, even a small increase in field will raise the local current density in the filament and the column beneath it substantially. As each pulse extends the filament deeper into the varistor, the field and current density beneath the filament will increase until eventually the entire fixed current from the tester will be flowing in the filament. This concentration of field and current increases the Joule heating along the column below the filament. It is not surprising that, under some circumstances, temperature rises can occur large enough to melt, vaporize and fracture the ZnO.

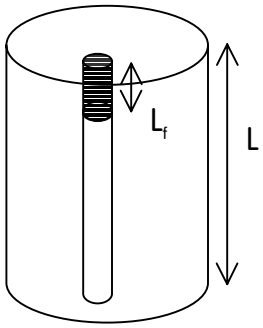

Figure 8. Schematic illustration of a conductive filament (shaded) in a partial breakdown varistor.

Before quantifying the consequences of this model, I first examine the correctness of the assertion that the enhanced current density at the filament tip will stay mostly contained in the column beneath, rather than spread into the bulk of the varistor. Indeed, as shown in App. B, if the varistor conductivity were independent of electric field, then the current would spread into the bulk.[6] However, in the switching regime, the conductivity of varistor material increases with increasing current density. This is a positive feedback effect – increased current density locally makes it more favorable to conduct current through the same locality. The effect is the same as replacing the varistor material in the column with a rod of more conductive material. Current localization under a conductive electrode protrusion has been graphically demonstrated using a two-dimensional resistor lattice model in which the resistors were assigned nonlinear properties similar to varistors.[7] A small amount of current spreading is also seen in those calculated results.

Model Electrical Effects

While there may be some spreading of the current density beneath the filament tip, we will ignore it to calculate approximately the voltage decrease due to the filament. Using the subscripts b and c to denote the varistor bulk and column beneath the filament, respectfully, we can first write the equation for the current distribution.

$$I = J_b A_b + J_c A_c = A_b p E_b^{\alpha} + A_c p E_c^{\alpha} = A_b p E_{b0}^{\alpha} + A_c p E_{c0}^{\alpha}, \quad (3)$$

where A is the cross-sectional area and the subscript 0 denotes the initial, no filament condition. Using $a = A_c/A_b$ and $\ell = L_f/L$, and noting that

$$E_{b0} = E_{c0} \text{ and } E_c = E_b L/(L - L_f),$$

the measured voltage as a function of filament length can be written as

$$V(\ell)/V_0 = (1 - \ell)\{[1 + a]/[(1 - \ell)^{\alpha} + a]\}^{1/\alpha}. \quad (4)$$

The varistors tested had 5 mm diameters, so filament diameters of 20 μm and 200 μm yield $a = 1.6 \times 10^{-5}$ and 1.6×10^{-3}, respectively. The curves for these two ratios are given in Figure 9. Notice that both have the same basic shape as the data in Figure 2. This suggests that they be fit

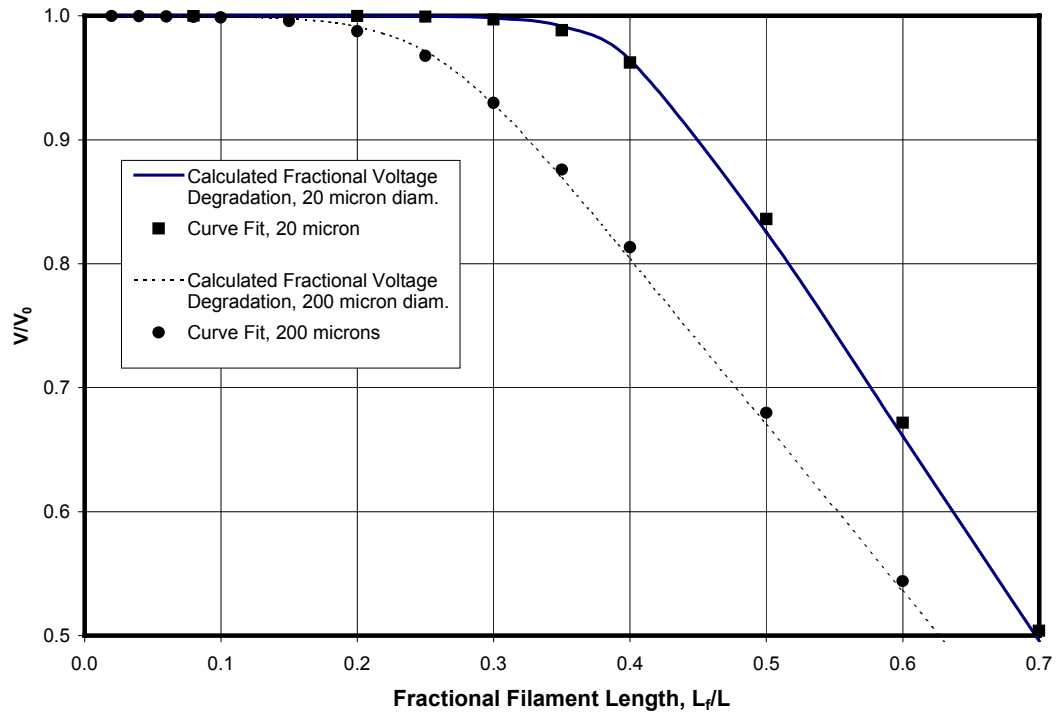

Figure 9. Calculated voltage degradation as a function of filament length from Eq. (4). Also shown as data points are the fits to the calculations represented by Eqs. (5) and (6).

to the same functional form as Equation (2). The calculated values of V/V_0 versus ℓ are well approximated by

$$V(\ell)/V_0 = 1 - 0.06\ell n\{1+\exp[(2/3)(42\ell - 17)]\}, \text{ for a 20 } \mu m \text{ filament,} \quad (5)$$

and $$V(\ell)/V_0 = 1 - 0.06\ell n\{1+\exp[(2/3)(34\ell - 9)]\}, \text{ for a 200 } \mu m \text{ filament.} \quad (6)$$

The two curve fits are shown as points in Figure 9.

Model Thermal Effects

The nucleation and propagation of a conducting filament with successive high power pulses causes an increase in both electric field and current density at the filament tip, which increases the local Joule heating per unit volume, $J \cdot E$, significantly. The details of the calculation for the corresponding temperature rise during a single pulse have been relegated to Appendix A. Here we provide a summary of the pertinent issues for the varistors tested.

The standard high current for the reliability tests was $I_0 = 2.2$ A, which corresponds to $J_0 = 11$ A/cm^2 when distributed uniformly through undamaged varistors with no filaments. The value of the varistor's switching field in this uniform current density is $E_0 = 40$ KV/cm. As shown in Appendix A, this uniformly distributed electrical power heats the varistor at a rate of 0.16 K/μs, and thus $\Delta T = 1.6$ K by the end of the 10 μs pulse. However, when a filament forms, the local current and field at the tip increases and the local temperature rise is much higher. The temperature increase in the column beneath the filament depends on the power per unit length, $Q_f = E \cdot I = E \cdot J \cdot A_c$, where A_c is the cross-sectional area of the column. The factor by which Q_f is increased from the uniform value can be determined from the relations derived in the electrical section above.

$$Q_f(\ell,a)/Q_{f0} = J_c E_c / J_{c0} E_{c0} = (E_c/E_{c0})^{\alpha+1} = \{E_b/[(1-\ell)E_{b0}]\}^{\alpha+1}. \quad (7)$$

Using Eq. (4) this can be written as:

$$Q_f(\ell,a)/Q_{f0} = \{[1 + a]/[(1 - \ell)^{\alpha} + a]\}^{1+1/\alpha}. \quad (8)$$

As ℓ grows, the first term in the denominator begins to get small rapidly, which increases the ratio. Using the calculated results from Table A1 and the thermophysical parameters of Table A2, the temperature increase by the end of the 10 μs pulse can be estimated. Shown in Figure 10 are the temperature increases at the tip after 10 μs of applied current for filament diameters of 20, 100, and 200 μm. The dependence on filament length simply reflects the fact that both E and J increase at the tip as the filament grows longer. The small filament diameters concentrate J the most and thus their columns have the highest temperature rise. The saturation of ΔT for the 200 μm filament reflects the fact that essentially all varistor current is flowing in the filament for $\ell > 0.4$. Note also that because the filament is assumed to be conductive, there is little or no field in the filament, and thus its heating is negligible.

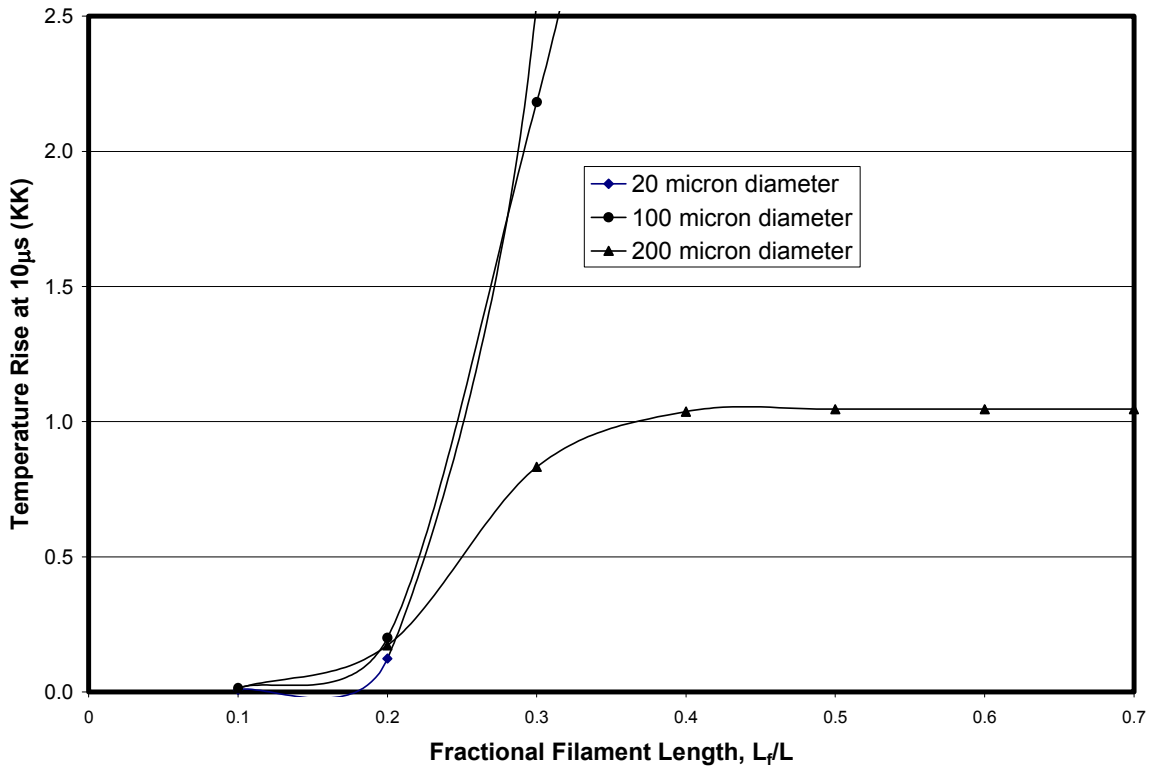

Figure 10. Filament tip temperature rise in kilokelvins at the end of a 10 μs high power pulse. Calculated increases are shown for three filament diameters. The amount of increase depends on the extent of filament penetration, L_f/L, because of the consequent concentration of Joule heating at the tip.

For ZnO, the melting point is nearly 2000ºC ($\Delta T = 2.0$ kK) and the temperature at which the vapor pressure[8] reaches 1 atm. is about 1700ºC ($\Delta T = 1.7$ kK). The model calculations indicate that both temperatures are exceeded for filaments less than 200 μm in diameter once they have penetrated 30% of the varistor length.

Comparison of Model and Experiments

To connect the model electrical calculations with the single curve breakdown data, we assume that the filament length is proportional to the number of high current pulses received after the actual start of breakdown,

$$\ell = kP_b \tag{9}$$

where k is the constant of proportionality. Note that this may not be a good assumption near the beginning of degradation when the filament may propagate slower because of lower stimulus (thermal or electrical). Next we note that because of the noise in the voltage measurements, we may not observe the actual start of breakdown. It is only after the voltage has decreased by

about 1% that it becomes apparent that the monotonic breakdown is underway. Thus it makes sense to write

$$P_b = P_a + P_h, \tag{10}$$

where P_a is the number of pulses applied since the evidence of breakdown becomes apparent and P_h is the "hidden" number of pulses applied after nucleation, but before breakdown is noticed using the Sandia tester. With these two assumptions, we can now equate Equations (2) and (5) to obtain k = 0.024 and P_h = 11 for a 20 μm filament. For a 200 μm filament, Equations (2) and (6) yield k = 0.029 and P_h = 3. Taken literally, this means that each pulse during the breakdowns shown in Figure 2 is advancing the filament length 2½% of the total varistor length, for either diameter filament. The P_h value implies that the actual start of breakdown and filament formation may be occurring 3 to 11 pulses before it is reliably noticed in the voltage output of the tester. So without knowing the diameter of the filament, it is difficult to tell whether different pulse breakdown delays among the tested samples are differences in nucleation time or filament diameter.

As a test of the model, seven varistors were pulsed to various values of V/V_0. All seven varistors followed the single curve breakdown of Fig. 2, and none of them had surface tracks or fractures. After the initial pulsing they were cut to different lengths to look for electrical and structural evidence of breakdown. The idea is illustrated in Figure 11. Depending on the degree of breakdown, the rods were cut into either two or three pieces with the intent to have one of the pieces not penetrated by the filament. The cut surfaces were examined for holes. Finally each cut face was given an electrode of silver paint and each piece was electrically re-tested using the same current. The electrical results are summarized in Figure 12.

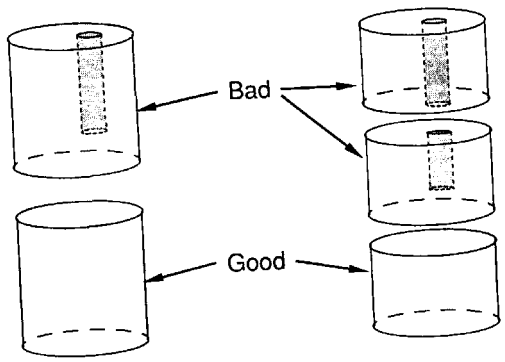

Figure 11. Illustration of how rods were sectioned to determine filament penetration.

Figure 12 is a composite of data from this sectioning experiment plus the 200 μm calculated curve of Figure 9, both plotted as fractional degraded voltage versus fractional length. The voltage axis of V/V_0 has the same meaning for each, but the abscissa denotes different quantities. For the calculated curve, it is the predicted length of the filament. For the data, it is the fractional length of the cut(s) from one varistor electrode. The superimposed drawings illustrate both the experimental cut locations and the calculated filament length (associated with the arbitrary placement of the drawing on the voltage axis).

Consider first the five varistors whose breakdown was limited to $V/V_0 > 0.75$. These were all cut approximately into halves. Four of the five varistors (triangles) each contained one half-piece with very low voltage on the first re-test pulse. The other half-piece exhibited a constant switching voltage through 25 additional pulses that corresponded to the initial electric field in the

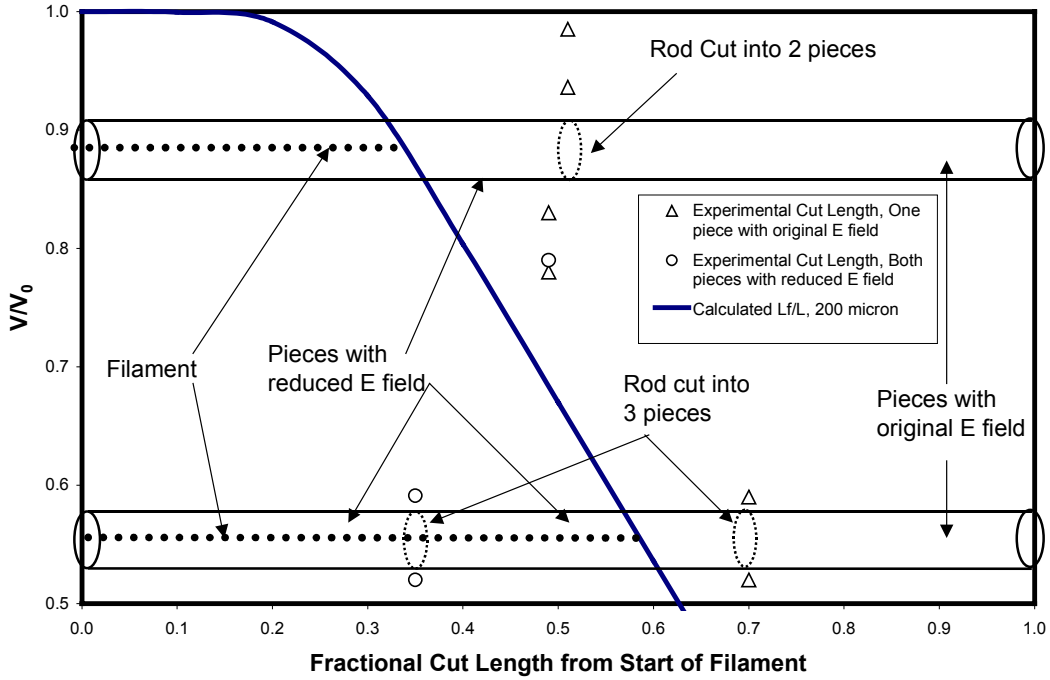

Figure 12. Test of filament length prediction for degraded varistors. The solid curve is a replot of the 200 μm calculation in Figure 9. Also plotted as open symbols are data from 7 varistors that were pulsed to various levels of breakdown as indicated by their position on the voltage axis. The symbol location on the length axis shows the length of sections cut subsequent to the breakdown. Circles indicate that pieces on both sides of the cut were electrically degraded, and triangles indicate that a piece on one side of the cut was degraded but the other piece was not. Superimposed are schematic drawings of the varistor rod showing the two types of sectioning used. They are located in the voltage range appropriate for each type, and the dashed line graphically shows the filament length of the calculation.

varistor. In other words, one half piece was catastrophically broken down electrically while the other half was a perfectly good varistor with an un-degraded switching field. None of these samples showed holes or halo pits on the electrode or cut surface prior to re-test. For the fifth varistor in this group (circle) both halves exhibited catastrophic electrical breakdown upon re-test, one on the first tester pulse, and one on the second. This sample had a halo pit on both cut surfaces prior to re-test.

The remaining two varistors were degraded to $V/V_0 < 0.6$ and were cut roughly into thirds. Each of these varistors had two adjacent pieces that were badly degraded and broke down immediately on re-test. The third piece of each varistor was just like new, exhibiting the original switching field on re-test. However, after several pulses, each good third developed a breakdown initiated at the edge of the silver paint spot that did not cover the entire cut surface. Although these two varistors were electrically similar, there was a major structural difference between them. The varistor that was degraded to V/V_0 of 0.52 had no apparent sign of a breakdown track or halo on its cut surfaces. The varistor degraded to 0.59 had a track that

completely penetrated the cathode third, from electrode to cut, and entered the middle third from the cut.

Conclusions

A major assumption of the model is that breakdown is due to a conducting filament originating at one of the electrodes. The strongest evidence in support of this assumption comes from the sectioning experiments. These experiments show that the degraded, high conductivity region is localized to one end of the rod, while the other end shows no evidence of degradation. Also in all cases in which a breakdown track was observed, it had one end at an electrode. Thus, confirmation of the electrode-initiated part of the assumption rules out a uniform bulk degradation.

The filamentary nature of the breakdown is only partially proven. Electrically, the linear decay of V/V_0 with successive pulses is not proof of a thin filament since a conducting region comprising the whole rod cross-section (a filament of the whole) would produce the same linear decay. Only a small fraction of the varistors had tracks as visible evidence of a filament. In addition, the observation of the Bi-halos in a few other rods might be interpreted as a remnant of a hot filament. Eda, in his paper[9] on varistor destruction (catastrophic breakdown), notes that intergranular Bi_2O_3 melts at 820ºC. Thus a filament reaching this temperature might cause the Bi_2O_3 to melt and agglomerate differently.

There may be several reasons why structural evidence for filaments has not been seen in many of the electrically degraded varistors. One reason might be the diameter of the filament. As seen from the curves in Figure 10, filaments with diameters greater than 200 μm are not expected to raise the local temperature enough to vaporize or melt the ZnO and thus cause a track. Even for smaller filaments, the large local temperature increases do not occur until the filament has propagated 20% of the rod length. Since the filament itself is conductive, its Joule heating is always small. So for penetration beyond 20%, the hot tip is capped by a cooler, solid plug of filament, which may prevent venting or other gross structural changes. In fact, this latter situation both explains why tracks often have associated fractures and confounds explanation for the few cases in which tracks formed without fractures.

Nevertheless, a thin filament is the most likely form of the changed material. As noted at the end of the Breakdown Model section, a conductive filament, once formed by any cause, will tend to concentrate the current into the material beyond its tip because of the nonlinear properties of the varistor. In that sense, filaments are stable, self-propagating structures. However, their propagation through the varistor does not appear to be primarily driven by heating at the tip. As noted in the last paragraph, short filaments of almost any sensible diameter are incapable of concentrating enough current to provide significant heating during the pulse. If temperature is not the primary cause, then the propagating degradation must be due to electrical effects.

Speculations on Filament Initiation

As stated earlier in the section titled *Pulse Test Results – Electrical*, most of the varistor samples tested did not show electrical degradation or breakdown. Although 25 high voltage

pulses was a standard test, many were tested up to 50 pulses. A few were tested to hundreds of pulses, one through 800 pulses, with no sign of degradation. From these results, one may reasonably conclude that the inherent reliability of the varistor material is excellent for the electric field and current density used. The observed failures were likely caused by a flaw in the material as in other failure mechanisms, such as mechanical fracture. As argued above, the initiating flaws are most likely on or near one of the electrode faces, and it is some type of electrically conducting protrusion. This probability was also expressed by Vojta and Clarke[7] who used a variable resistor network to do computational simulations of varistor conduction in two dimensions. They showed that conductive inclusions at an electrode cause more current concentration than the same inclusions in the body of a varistor but separated from an electrode surface. They concluded that "electrode protrusions … are likely sources for failure."

Mechanistically, how can an electrically conducting protrusion initiate degradation? Evidence above shows that it is unlikely to be a thermal mechanism from Joule heating. A more likely possibility is the increased local electric field associated with the shape of the protrusion. As an example, the electric field due to a hemisphere-shaped protrusion is calculated in Appendix B. At the tip of the protrusion, the local electric field is three times the uniform field far away. This increase is independent of the diameter of the protrusion (for diameters small compared with the lateral extent of the medium).

The increased electric field will not only increase the current during the applied pulse, but also may change the permanent conductivity of the varistor material. The current increases during the pulse are entirely electronic. The current-voltage characteristics of varistors are determined by electrostatic potential barriers that form at the ZnO grain boundaries, as shown by the simplified schematic of Figure 13. These barriers substantially impede electron flow at low voltages. As the voltage is increased, the barrier lowers and electrons can more easily transit. Because the current depends exponentially on the barrier height, small changes in voltage can result in large current changes which gives rise to the switching (or regulating) phenomena. However, the [energy] height and [depletion layer] width of these electrostatic potential barriers are determined by the density of lattice defects or impurities near the grain boundary that can be ionized to a positive charge state. If the density of these lattice sites changes, then the equilibrium potential barrier and its response to voltage will change permanently. The positive charges may be induced to electro-migrate due to the increased field and high current. Sensitivity of the equilibrium barrier height, Φ_B, to the density of positive charge in the depletion region, N_d, can be estimated assuming that the total charge per unit area at the boundary, Q, does not change. The relationship is[10]:

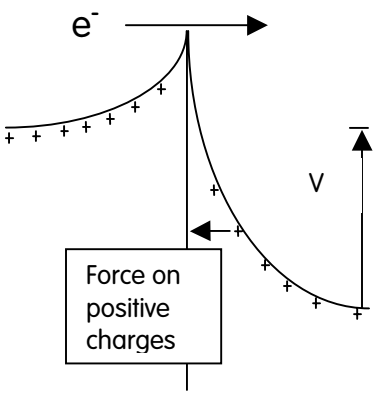

Figure 13 – Schematic diagram of a grain boundary electrostatic barrier under an applied voltage, V.

$$Q = 2(2\varepsilon\varepsilon_0 N_d \Phi_B)^{1/2}.$$

In this equation ε and ε_0 are the relative and free space dielectric constants, respectively. So for constant Q, if N_d doubles, then the barrier height reduces by a factor of two. This may account for the higher conductivity of the varistor material at the tip of the protrusion or filament.

What would constitute an electrically conductive protrusion at an electrode surface? Clearly, a physical depression into which the silver-loaded epoxy was pressed would qualify. Such a depression could form during surface grinding due to grain pull-out or preferential erosion in a porous region. Possibly the depression could just be a pore exposed at the surface. Another, more insidious, possibility for the protrusion might be the presence of excess Bi_2O_3 at the surface. Bismuth oxide has been reported to be conductive[11], so a continuous phase from the surface into the bulk would also act as a protrusion. This type of concentrated Bi_2O_3 has been observed in some batches of varistors in the form of "bismuth halos" discussed above in the section titled *Pulse Test Results – Structural* and shown in Figure 6.

Acknowledgements

The author is pleased to acknowledge the assistance of Robert Jaramillo in the electrical testing, and Lori Maestas for the electron microscopy and special sample preparations. Jim Voigt and Steve Lockwood have been especially helpful in discussing powder and rod preparation issues.

Appendix A: Thermal Calculations

This appendix describes the calculation of temperature rise for cylindrical filaments of material, first generally and then specifically for ZnO. Here also are gathered various thermal parameters for ZnO.

General Solution

The general problem solved here is the temperature rise in a cylinder of radius, R_f, heat capacity per unit volume of $\rho_f c_f$, and infinite thermal conductivity. The cylinder is embedded in a semi-infinite medium of heat capacity per unit volume of $\rho_m c_m$ and thermal conductivity of κ_m. Initially the filament and medium are at the same temperature. Beginning at time zero the filament is heated by a power of Q_f per unit length. Carslaw and Jaeger[12] give the solution in terms of a dimensionless temperature increase, $(\kappa_m \Delta T/Q_f)$, and time, (t/τ_m):

$$\frac{\kappa_m \Delta T}{Q_f} = \frac{2\alpha_1^2}{\pi^3} \int_0^\infty \frac{\left[1 - e^{-(t/\tau_m)u^2}\right] du}{u^3 \Delta(u, \alpha_1)}, \qquad \text{(A1)}$$

where $\Delta(u, \alpha_1) = [uJ_0(u) - \alpha_1 J_1(u)]^2 + [uY_0(u) - \alpha_1 Y_1(u)]^2$,

and $\alpha_1 = 2\rho_m c_m / \rho_f c_f$ = twice the ratio of heat capacities,

and $\tau_m = (\rho_m c_m / \kappa_m) R_f^2$.

The integral was solved numerically using numerical approximations to the various Bessel functions. The results are tabulated below, and shown graphically in Figure A1.

t/τ_m	$(\kappa_m/Q_f)\Delta T$	Adiabatic
0.01	2.65E-03	3.18E-03
0.02	5.07E-03	6.36E-03
0.0316	7.68E-03	1.00E-02
0.04	9.45E-03	1.27E-02
0.06	1.34E-02	1.91E-02
0.08	1.70E-02	2.54E-02
0.10	2.04E-02	3.18E-02
0.20	3.48E-02	6.36E-02
0.316	4.82E-02	1.00E-01
0.40	5.64E-02	1.27E-01
1.00	9.78E-02	3.18E-01
3.16	1.69E-01	1.00E+00
10.00	2.54E-01	3.18E+00

Table A 1 Dimensionless temperature increase in the cylinder vs dimensionless time from the general equation and calculated adiabatically.

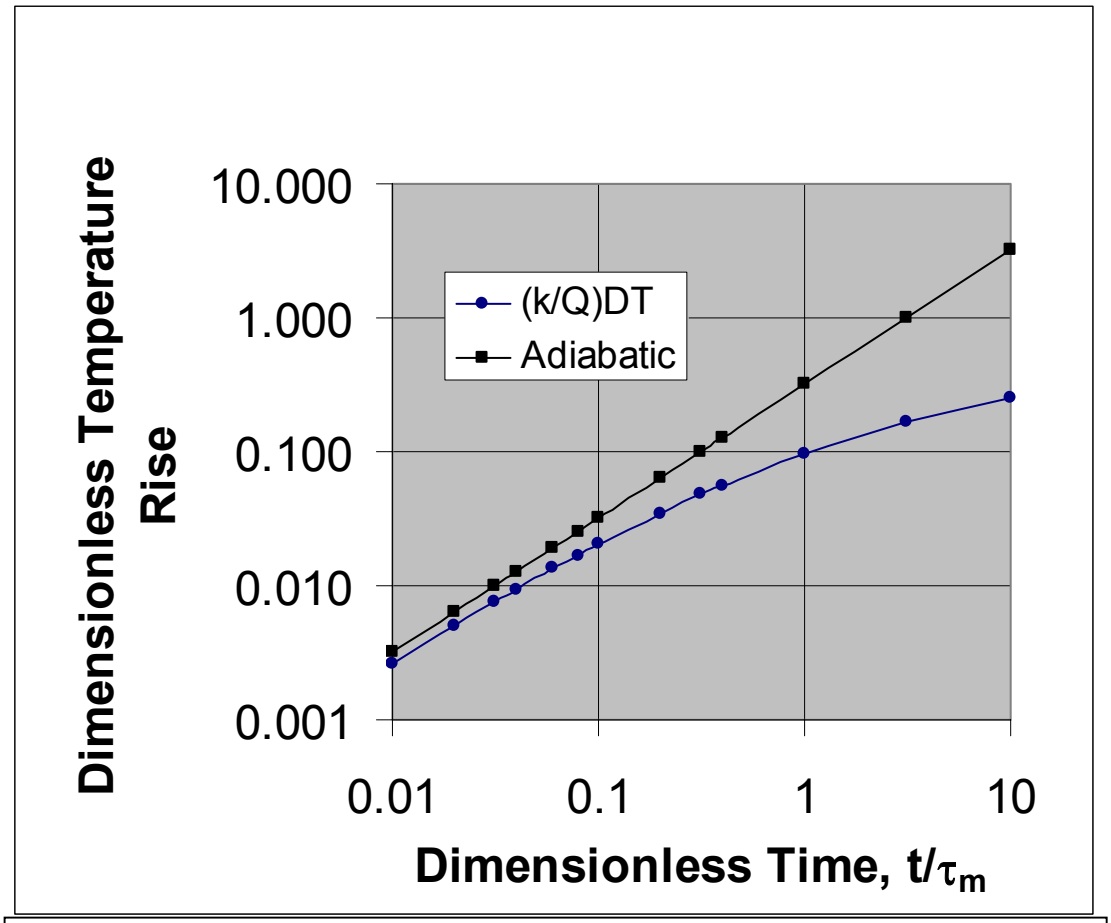

Figure A 1 Graph of filament temperature increase vs time for embedded and adiabatic conditions. The embedded solution used $\alpha_1 = 2$.

The temperature increase of the filament heated under adiabatic conditions is given by:

$$\Delta T = (Q_f/\rho_f c_f \pi R_f^2)t. \qquad \text{(A2)}$$

Note that for $t << \tau_m$, the general solution for the embedded filament is also linear in t, so

$$(\kappa_m/Q_f)\Delta T = Xt/\tau_m = Xt\kappa_m/(\rho_m c_m \pi R_f^2),$$

where X is a constant of proportionality. Now in the limit of $t \rightarrow 0$, the filament and surrounding medium are at the same temperature. With no temperature difference, there is no heat flow to the medium, and the temperature rise is essentially adiabatic. This fixes the constant of proportionality to be $X = \rho_m c_m/\pi\rho_f c_f$ and allows the adiabatic rise to be tabulated and plotted with the embedded data. This limiting condition simplifies the calculation of ΔT for $t << \tau_m$.

Temperature Increases in ZnO Varistors

To use the calculations above for the case of ZnO varistors, the thermophysical parameters of ZnO must be known. The Table A2 below lists them.

Material	T (ºC)	κ[13] (W/m·K)	c[8] (J/g·K)	ρ (g/cm^3)	P_{vapor}[8]
ZnO	20		0.50	5.6	
	200	17			
	227		0.58		
	627		0.64		
	800	5.3			
	1400				1
	1500				12
FC-77[14]	20	0.063	1.05	1.78	
Epon 828[15]	20	0.16	1.97	1.20	
Epon 828 w/GMB[15]	20		1.59	0.87	

Table A 2 Thermophysical parameters of ZnO, tester fluid, and encapsulants.

From these parameters one can compute the time constant, τ_m, from the expression below Eq.(A1) above. It is difficult to give a precise meaning to the time constant, τ_m, because the thermal problem involves diffusive heat transfer which is not a simple exponential relationship. However, as a rough approximation, one can state that for $t < 0.1\tau_m$ heating is nearly adiabatic, and that after the heating is stopped, the excess temperature is reduced by 50% at $t = 0.1\tau_m$.

Filament Radius	10 μm	50 μm	100 μm	2.5 mm
τ_m (room temp.)	17 μs	0.43 ms	1.7 ms	1.0 s
τ_m (high temp.)	67 μs	1.7 ms	6.8 ms	4.2 s

Table A 3 Thermal time constants for ZnO surrounding filaments of various radii.

As can be seen from the two tables above, the temperature increase in all but the very smallest filaments can be calculated adiabatically for pulses limited to 10 μs in duration. Using the room temperature thermophysical parameters for the whole varistor rod (2.5 mm radius) as the filament, in any of its various environments, the rise is 0.16 K/μs for conditions of the high current pulse, J = 11 A/cm^2 and E = 40 KV/cm.

Appendix B: Electrical Protrusion Calculation

Presented here is a simplified version of the more general solution for the effect of inhomogeneities on electric field, current density, and power dissipation distributions in a conducting medium[6]. For a perfectly conducting sphere of radius R in a medium of uniform and isotropic conductivity σ_m, the electric field outside the sphere is given by[16]

$$\mathbf{E}/E_0 = \mathbf{u}_r[1 + 2(R/r)^3]\cos\theta - \mathbf{u}_\theta[1 - (R/r)^3]\sin\theta, \qquad \text{(B1)}$$

where bold indicates vectors and $\mathbf{u}_r$ and $\mathbf{u}_\theta$ are the radial and azimuthal unit vectors, respectively, in spherical polar coordinates. The uniform field, $\mathbf{E}_0$, far from the sphere defines the direction of the pole at $\theta = 0$, and r is the distance from the center of the sphere. The field magnitude is

$$E = \{1 + 2(R/r)^3(3\cos^2\theta - 1) + (R/r)^6(3\cos^2\theta + 1)\}^{1/2}E_0, \qquad \text{(B2)}$$

At the surface of the sphere, r = R, the field is strictly radial and its magnitude reduces to $E = 3E_0\cos\theta$. The streamlines of the electric field, and hence the current, are found by solving the vector cross-product equation

$$[\mathbf{E(r)}/E(\mathbf{r})]X d\mathbf{r} = 0, \qquad \text{(B3)}$$

where d**r** is an incremental change in position of the vector **r**. This equation was solved numerically with representative results shown in Figure B1.

The conducting sphere concentrates current that eventually spreads into the surrounding medium. The streamlines show the current paths, but not the magnitude of the current density. However, from Eq. (B2) one can calculate that maximum current density drops from $3\sigma_m E_0$ at r = R to only $1.07\sigma_m E_0$ at r = 3R for this constant conductivity medium.

Although this calculation of electric field is for a perfectly conducting sphere in a uniformly conducting medium, the symmetry of the configuration also allows interpretation as the electric field produced by a perfectly conducting hemispherical protrusion from an otherwise flat conductive interface at Z = 0. For a varistor rod, this corresponds to one electrode with a hemispherical indentation that is filled with the silver-loaded epoxy.

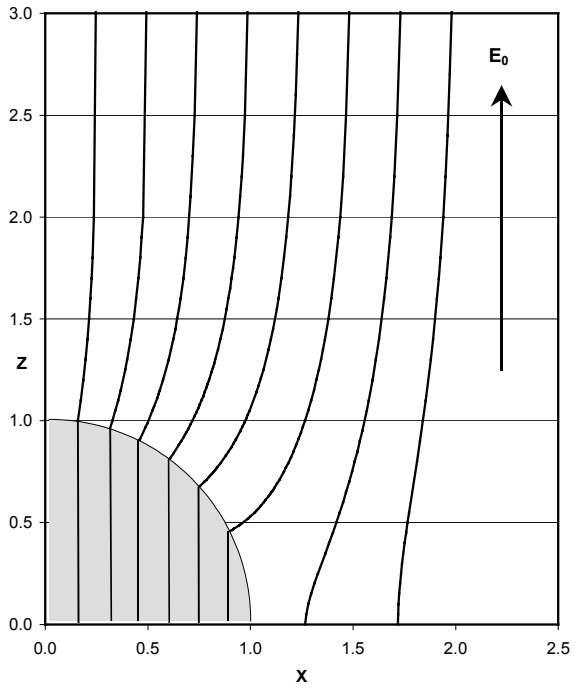

Figure B1 – Streamlines from a perfectly conducting sphere in a uniform electric field. For this graph, R = 1, and only one quadrant is shown because of symmetry about the z-axis.

References and Notes

[1] R.G. Dosch, B.A. Tuttle, and R.A. Brooks, J.Mat. Res. **1** (1986)90.

[2] T.J. Gardner and S.J. Lockwood, Sandia Report SAND87-2194, "Scale-up of a Batch-Type Chemical Powder Preparation Process for High Field Varistor Fabrication."

[3] The current is not truly fixed throughout the pulse testing. It increases slightly as the varistor degrades in switching voltage. For all tests reported here the increase was a factor of two or less. With the high value of the nonlinearity coefficient this causes only a small increase in voltage relative to the true fixed-current value. Because of uncertainties in the procedure for correcting the voltage, all voltages plotted are those actually measured and not corrected.

[4] A two-dimensional version of this model, but without the pulse-advancing feature, was borrowed from an unpublished memo of the author, with his permission, by A. Vojta and D.R. Clarke, (J. Appl. Phys. **81**(1997)985) and used to simulate current flow in varistors.

[5] There are really two factors that enhance the electric field below the tip. One is due to the gross penetration of the filament which drops the electrode voltage over a reduced length. There is also a local increase due to the shape of the tip. For a hemispheric protrusion from one electrode, the field at the bottom of the protrusion is three times the uniform field, and the integrated current increase is three times the uniform current through the same cross-section. This is covered in more detail in Appendix B and the report section on breakdown initiation. For the model calculation of the degraded voltage the local effect will be neglected, partly because the exact shape of the tip is not known and partly because the essential (if only approximate) phenomena are described by the gross penetration alone.

[6] J. Helsing, J. Axell, and G. Grimvall, Phys. Rev. B **39**(1989)9231. This paper shows how to calculate the electric field and hence current in a material containing a spherical conducting inhomogeniety. By symmetry this can be viewed as a special case of the conducting filament as a hemispherical protrusion from the top electrode. At a distance of two hemisphere radii from the protruding surface, the current density is nearly uniform everywhere.

[7] A. Vojta and D.R. Clarke, J. Appl. Phys. **81**(1997)985.

[8] ZnO values from SOLID STATE PHYSICS, ed. F. Seitz and D. Turnbull (Academic Press, NY, 1959) vol. 9, "Electronic Processes in Zinc Oxide."

[9] K. Eda, J. Appl. Phys. **56** (1984) 2948.

[10] G.E. Pike and C.H. Seager, J. Appl. Phys. **50** (1979) 3414

[11] H.A. Harwig and A.G. Gerrards, J. Sol. St. Chem. **26**(1978)265.

[12] CONDUCTION OF HEAT IN SOLIDS, H.S. Carslaw and J.C. Jaeger (Clarendon, Oxford, UK, 1959, 2nd ed., Chapter XIII, pg. 344, Eq. (8).

[13] ZnO values from AMERICAN INSTITUTE OF PHYSICS HANDBOOK, (McGraw-Hill, NY, 1972) 3rd ed., pg. 4-159.

[14] All FC-77 values from Chemical Products Division, 3M Company.

[15] All Epon 828 values from: Encapsulating Resins Properties Chart, A.J. Quant and C.W. Hatcher, Sandia Labs., May 1971.

[16] AMERICAN INSTITUTE OF PHYSICS HANDBOOK, (McGraw-Hill, NY, 1972) 3rd ed., pg. 5-23.

Distribution:

MS 0328		James Wilder, 2612
MS 0328		Russell Humphreys, 2612
MS 0515		Jeffrey Keck, 2561
MS 0515		Robert Stiers, 2561
MS 0515		Todd Haverlock, 2561
MS 0515		Doyle Morgan, 2561
MS 0515		Steven Barnhart, 2561
MS 0521		Richard Pike, 2561
MS 0521		Timothy Scofield, 2561
MS 0521		Frank Bacon, 2502
MS 0885		Michael Cieslak, 1801
MS 0885	(5)	Gordon Pike, 1801
MS 0888		Robert A. Anderson, 1846
MS 0889		S. Jill Glass, 1843
MS 0959		Steven J. Lockwood, 14192
MS 0959		Pin Yang, 14192
MS 0959		Jon Munford, 14192
MS 1152		Mark Kiefer, 1642
MS 1153		Guillermo Loubriel, 15333
MS 1349		William F. Hammetter, 1846
MS 1411		Nelson Bell, 1843
MS 1411		Duane Dimos, 1843
MS 1411		Bruce Tuttle, 1846
MS 1411		James Voigt, 1843
MS 1413		Carleton Seager, 1111
MS 9018		Central Technical Files, 8945-1
MS 0899	(2)	Technical Library, 9616
MS 0612	(1)	Review & Approval Desk, 9612 For DOE/OSTI